HHS Public Access

Author manuscript

ACS Sens. Author manuscript; available in PMC 2025 March 22.

Published in final edited form as:

ACS Sens. 2024 March 22; 9(3): 1372–1381. doi:10.1021/acssensors.3c02383.

Waste Coffee Ground – Derived Porous Carbon for Neurochemical Detection

Blaise J. Ostertag[1], **Ayah J. Syeed**[1], **Alexandra K. Brooke**[1], **Kamya D. Lapsley**[1], **Evan J. Porshinsky**[1], **Ashley E. Ross**[1,*]

[1]University of Cincinnati, Department of Chemistry, 312 College Dr., 404 Crosley Tower, Cincinnati, OH 45221-0172, USA

Abstract

We present an optimized synthetic method for repurposing coffee waste to create controllable, uniform porous carbon frameworks for biosensor applications to enhance neurotransmitter detection with fast-scan cyclic voltammetry (FSCV). Harnessing porous carbon structures from biowastes is a common practice for low-cost energy storage applications; however, repurposing biowastes for biosensing applications has not been explored. Waste-coffee ground (WCG)-derived porous carbon was synthesized by chemical activation to form multi-void, hierarchical porous carbon, and this synthesis was specifically optimized for porous uniformity and electrochemical detection. These materials, when modified on carbon-fiber microelectrodes, exhibited high surface roughness and pore distribution which contributed to significant improvements in electrochemical reversibility and oxidative current for dopamine (3.5 ± 0.4 – fold) and other neurochemicals. Capacitive current increases were small showing evidence of small increases in electroactive surface area. Local trapping of dopamine within the pores led to improved electrochemical reversibility and improved frequency independent behavior. Overall, we demonstrate an optimized biowaste-derived porous carbon synthesis for neurotransmitter detection for the first time and show material utility for viable neurotransmitter detection within a tissue matrix. This work supports the notion that controlled surface nano-geometries play a key role in electrochemical detection.

Graphical Abstract

*Corresponding author: Ashley.ross@uc.edu.

Supporting Information

We provide additional surface characterization and experiments to support the claims within this manuscript. The surface characterization included involves further SEM imaging of the tip of a porous carbon – modified CFME and Raman D/G analysis of the four synthesized porous carbon materials. Analysis of the redox cycling ratio was included to show the extent to which local trapping at these porous carbon geometries reduced dopamine-*o*-quinone desorption. Capacitive current analysis was included to show minimal increases in non-faradaic current following modifications due to non-uniformity. A survey of other important neurochemicals is shown. Lastly, frequency dependent analysis was provided to investigate the percentage of normalized current loss at a scan repetition frequency of 100 Hz.

Conflicts of Interest

The authors declare no conflicts of interest.

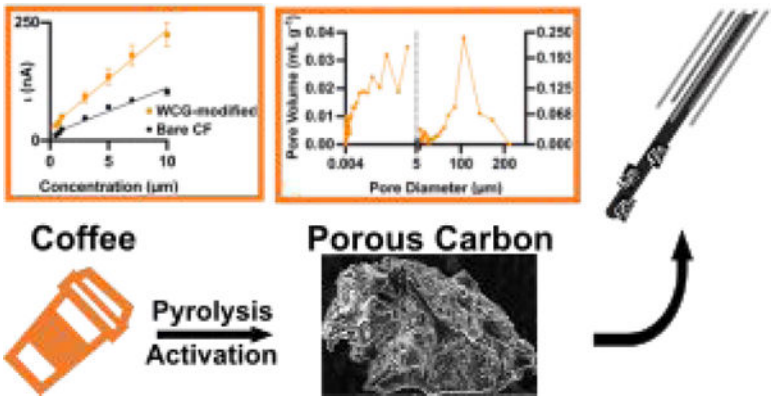

Keywords

porous carbon; recycled waste; electrochemistry; sensors; biomass; voltammetry

Here, we synthesized coffee waste-derived porous carbon material as novel electrochemical probes for real-time neurochemical detection with significantly improved sensitivity, redox cycling capabilities, and temporal resolution. Porous carbon material popularity stems from large surface areas and excellent catalytic properties suiting energy storage and reusability applications.[1–4] Routinely, porous carbon is synthesized to achieve carbon material pore size distributions. Approaches include chemical activation to achieve nanoporosity,[5,6] copolymerization methods for nano or micro-porous frameworks,[7–9] and, more recently, using green chemistry in an environmentally friendly manner.[10,11] Commonly, biowastes in the form of wood, coal, bone, and even coffee are cost-effective materials used to create porous carbon materials. Although these biowaste-derived porous materials consist of several properties sought after for electrochemical biosensing,[12] to date, they have not been investigated for this purpose.

Neurochemical sensing in real-time is a popular application of new electrochemical probes, most commonly using the technique fast-scan cyclic voltammetry (FSCV). Traditionally, FSCV uses carbon-fiber microelectrodes (CFMEs) due to their biocompatibility, low detection limits, and small size[13]; however, CFMEs lack controlled surface chemistry for attractive neurotransmitter interfacial interactions. Prior reports have modified the surface of CFMEs with new chemical functionalities,[14] polymers,[15] and carbon nanomaterials;[13,16] however, modification of these surfaces with nanoporous carbon materials is limited. The influence of surface geometries has been greatly examined, noting that porous geometries promote greater degrees of surface roughness and can even exhibit thin-layer cell characteristics for redox cycling amplification.[17,18] Novel nanoporous geometries have recent applications in microelectrode frameworks in the form of carbon nanotube (CNT) yarns[17,19] or CFME surface modifications with other carbon nanomaterials. [13,20–22] CNT yarns possess fast electron transfer characteristics, ease of functionalization, and high conductivity for ultrasensitive dopamine and serotonin detection.[23–26] Porous carbon nanofibers, nanospikes, nanohorns, and nanocavity pipettes have all been explored as surface geometry modifications exhibiting enhanced electron transfer rates, surface defect site

abundance, and, in some cases, redox cycling.[13,20–22] Our lab fabricated porous carbon microfibers as a result of these materials with highly localized defect dense macropores enhancing electrochemical reversibility with many of the aforementioned electrochemical properties.[27] Although these materials have excellent properties, pore controllability is difficult and often involves rigorous synthesis procedures. Here, we optimized a porous carbon synthetic route from coffee waste to fabricate porous carbon modified CFMEs for ultrasensitive neurochemical detection providing a novel application of biowaste-derived porous carbon materials.

The concept of biowaste reusability has inspired syntheses from various sources to create honeycomb-like porous carbon nanostructures: most notably, waste coffee grounds (WCG). Recently, several research groups have taken advantage of WCG-derived hierarchical multi-void structures[28] for controllable porosity for high-yield performance supercapacitor and energy storage qualities. These hierarchical porous carbons have now made their way into Li-Se batteries[10] embracing improved electron transfer rates and ion diffusion confinement similar to the properties of nitrogen-doped porous carbon electrocatalysts in solar cell/steam applications.[6,29] WCGs have even branched into carbon quantum dot syntheses forming nanoporous graphene membranes for water pollutant cleanup applications[30] along with aiding in dopamine detection,[31,32] but biowaste materials have yet to be used as an implantable biosensor.

Biowaste-derived porous materials have greatly advanced the field and performance of cost-efficient energy storage and supercapacitor research, but here we have explored these materials as biological probes. Simple chemical activation procedures produce desirable porous geometries while maintaining reusability for the formation of a sensing medium. Porous geometries have been extensively studied in electrochemistry, and this work has shown that pores provide edge-plane enhancements known to increase neurotransmitter adsorption sites across and electrode's surface.[33–35] This work not only provides a new electrode material for neurotransmitter detection but also further supports the existing notion that electrode geometry can greatly influence electrochemical behavior.

Experimental Methods

See supporting methods for information on chemical reagents and animal experiment methods

Waste coffee ground – derived porous carbon synthesis

Porous carbon was derived synthetically from previously brewed Dunkin Donuts medium roast coffee grounds dried in an oven (Fisher Sci 100L Ovn Grvty, Thermo Scientific, Pittsburgh, PA) at 80°C for 24 hours. Brewed coffee grounds were then placed in a quartz process tube (Quartz Scientific, Fairport Harbor, OH, USA) within a tube furnace (Lindberg Blue M, Thermo Fisher Scientific, Asheville, NC, USA) and heated to 700°C in atmospheric conditions for at least 2 hours and left to cool. The carbonized material's mass was then measured (XSR105 DualRange, Mettler Toledo, Columbus, OH, USA) and ground with KOH for activation. KOH ratios to coffee grounds include 1:2 and 2:1 by weight. The mixture was placed back within a process tube connected to a compressed nitrogen cylinder

(Wright Brothers Inc., Cincinnati, OH, USA) and heated to at least 700°C for 2 hours for pyrolysis and annealing.

Fabrication and modification of carbon fiber microelectrodes

T-650, 7 μm carbon fibers were used to produce cylindrical CFMEs (Mitsubishi Rayon Co, LTD, Tokyo, Japan). Microelectrodes were fabricated by vacuum (Welch, Monroe, LA) aspirating carbon-fiber through a 1.2 mm x 0.68 mm x 4" glass capillary tube (A-M Systems, Sequium, WA) and pulled vertically with an electrode puller (PE-22, Narishige Scientific, Tokyo, Japan). Electrodes were cut to a length of 100–150 μm under a microscope (Fisher Science Education). Before using, electrodes were suspended in isopropyl alcohol for 10 minutes and backfilled with 1 M KCl.

When modifying CFMEs with waste coffee ground – derived porous carbon, three modification techniques were explored for CFME surface coverage optimization. Electrodeposition was performed using a common waveform scanning from −1.2 V to 1.5 V at 5 V/s and 1 Hz for 30 s. Drop casting was performed by dropping a 10 μL dispersion of WCG-derived porous material onto the CFME tip and dried at 60 °C. Dip coating was performed by suspending electrodes into the desired solution for 5-minutes and dried at 60°C. Solutions were prepared in Milli-Q water at 2 mg/mL and sonicated (QSonica, LLC model Q55, Newtown, CT). After deposition, electrodes were dried at 100°C.

Surface characterization

Standard surface characterization techniques were used to analyze the chemical and physical properties of WCG-derived porous carbon. Pore size analysis was performed in partnership with Particle Technology Labs (Downers Grove, IL, USA). Gas physisorption isotherms using nitrogen gas were performed for mesopore (2 – 50 nm) analysis. Mercury intrusion porosimetry was used for macropore (0.004 – 200 μm) analysis. The material's Raman spectra were collected with a Renishaw InVia Raman microscope (Guocestershire, UK) using an Ar-ion laser at 10% power excited at a wavelength of 633 nm. Qualitative assessment and visualization of the pore structures was performed using a scanning electron microscope (SEM) collected using an FEI XL30 SEM at an accelerating voltage of 5.00 kV.

Electrochemical characterization

Electrochemical characterization was performed by collecting fast-scan cyclic voltammograms using a WaveNeuro potentiostat with a 1 MΩ headstage (Pine Instruments, Durham, NC, USA), HDCV Software (UNC-Chapel Hill, Mark Wightman), and a National Instruments PC1e-6363 computer interface board (Austin, TX, USA). Electrodes were scanned from −0.4 to 1.3 V *vs.* a Ag/AgCl reference electrode and back at a scan rate of 400 V/s and a frequency of 10 Hz. Cyclic voltammograms (CVs) were background subtracted. All electrodes were tested using flow injection analysis at a 1 mL/min flow rate using a Fusion 100 Two-Channel Chemyx Syringe Pump (Stafford, TX, USA).

Statistics

Statistics were performed using GraphPad Prism V. 9.0 (GraphPad Software Inc., La Jolla, CA, USA) with statistically significant p-values found at a 95% confidence interval. Values

are reported as mean ± standard error of the mean (SEM), and electrode number (or slice number) is denoted by *n*.

Results and Discussion

Waste coffee ground – derived porous carbon synthesis

Waste coffee ground – derived porous carbon was synthesized following well-established carbonization, chemical activation, annealing, and pyrolysis methods to create various degrees of microporous frameworks with high surface roughness (Figure 1).[6,8,10,11,28] Initial heating at 700°C in air enables carbonization of WCG's by the expulsion of non-carbonaceous material. After carbonization, WCG's are mixed with KOH, a known carbon activation agent, and heated to 700–900 °C under a N_2 atmosphere for consumption of carbon by oxygen and alkali metal penetration and retraction[5] forming activated microporous carbon. Following this procedure (Figure 1), WCG – derived porous carbon was dip coated onto carbon-fiber microelectrodes (Figure S1) to enhance the electrochemical detection of dopamine using fast-scan cyclic voltammetry (FSCV). Changes in the porous carbon synthesis procedure impact the microporous uniformity effecting the improvements in electrochemical detection. Therefore, we demonstrate a comprehensive optimization of porous carbon synthesis for ideal electrochemical detection. To our knowledge, this is the first instance of WCG/biowaste – derived porous carbon synthesized material for implantable biosensor applications. Of note, the use of biomass in this work presents an environmentally friendly route to synthesizing porous carbon; although, the overall environmental impact of this work is low without the adoption of these processes in other biosensor applications.

Surface characterization of synthesized porous carbon

Raman Spectroscopy.—Raman spectroscopy is used to characterize the sp^2 and sp^3 hybridization of carbon to identify the presence of specific carbon structures.[36–38] Here, we used Raman spectroscopy to investigate four synthesized porous carbons in which carbonization time, WCG:KOH activation ratio, and activation heating temperature were varied. The following synthesis variations were used: initial carbonization times from 2 to 3 hours, WCG:KOH activation ratio from 1:2 to 2:1, and activation heating temperature from 700°C to 900°C. Commonly, the D band (~1350 cm^{-1}) provides insight into the degree of defects and surface oxidation for carbonaceous materials and the G band (~1580 cm^{-1}) is a direct representation of graphitic carbon. We characterized the degree of defects on the surface of the WCG – derived porous carbon by analyzing the ratio of the intensity of the D and G bands (I_D/I_G).[39,40] Analysis (Figure S2A) shows high degree of defects for all materials regardless of carbonization initial heating time, WCG:KOH, or activation heating temperature (Figure S2, Table 1, One-way ANOVA with Bonferroni Post-test, n = 6). It is proposed that defect increases are generated during the KOH activation process; however, we show that regardless of KOH composition or activation heating temperature the defect degree is not significantly impacted. High defect degrees are evident surface chemistry features for improving electrochemical detection, but adjusting synthetic parameters can have not only an impact on surface chemistry but also surface geometry across all synthesized porous carbon materials.

Raman spectral bands are a result of inelastic scattering from chemical bond vibrations, and the carbon spectral bands of interest are the superposition of multiple peaks; therefore, peak-fitting analysis was used to critically assess the disorder of the porous surfaces.[41,42] We report the presence of five bands in the 1000 – 1800 cm^{-1} range: D*, D, D", D', and G (Figure S3). The presence of the D' (~1615 – 1635 cm^{-1}) and D" (~1500 – 1550 cm^{-1}) bands illustrate the oxygen content present in graphitic carbon. Shifting of the D" band to lower wavenumbers correlates to decreased oxygen functionality.[41] With the appearance of the D" band at ~1505 cm^{-1}, we report low oxygen content in all synthesized WCG-derived porous carbon materials hinting that oxygen functionality is sacrificed at the high synthesis temperatures of porous geometries. This is likely due to the final heating procedure in an inert N_2 atmosphere not allowing for further oxidation during the annealing process. Lastly, we analyzed the crystallinity levels of the four materials by calculating the ratio of the intensity of the D" and G bands ($I_{D"}/I_G$). We found all materials, regardless of initial heating time, WCG:KOH, and activation heating temperature, to have a consistent $I_{D"}/I_G$, inferring the crystallinity of these materials is consistent even with changes in carbonization and activation procedures (Figure S2B). Although we do not report variability in the defect degree, oxygen content, or crystallinity we conclude that neurotransmitter detection benefits significantly from the pore sizes and uniformity of greater carbonization times, higher KOH composition, and higher activation temperatures. Pyrolyzed WCG, when annealed with KOH, is known to produce microporous frameworks. This process is kinetically driven and, when accelerated at higher temperatures, micropore destruction is common where micropores merge into larger macropore sizes causing surface area decreases attributed to the following activation reaction:[10]

$$4C + 6KOH \rightarrow 6K + 3H_{2(g)} + 2CO_{(g)} + 2CO_{2(g)}$$

Macropore sizes are more sought after for local trapping overcoming diffusion kinetics of neurotransmitters of interest.[10] These results indicate further that geometry is an important factor in electrochemical detection.

Scanning Electron Microscopy (SEM).—Morphological analysis was performed using SEM to understand both pore size/ uniformity of the WCG – synthesized porous carbon and the surface coverage of the material upon electrode modification. Investigating the surface morphology of the four synthesized materials (Figure 2) shows roughened material with a variety of pore structures. Extensive pore structures are more evident in synthesized materials with longer carbonization times while more KOH for activation (Figure 2C-D) produces pore geometries large enough for local trapping. Prior work estimates that pore sizes on the magnitude of the diffusion layer are needed for local trapping with enhanced electrochemical reversibility.[43] Here, we illustrate the presence of pores on the lower macropore scale by carbonizing for 3-hours at 700°C, 1:2 WCG:KOH, and activation at 700°C (Figure 2C) compared to larger macropores achieved by increasing the activation temperature to 900°C (Figure 2D).

Here, we investigated CFME modification techniques in which dip coating was determined optimal for dispersing porous carbon material on the surface with high S/N. More in depth

analysis on modification procedure analysis can be found in the following electrochemical characterization section. Following dip coating, we observe all materials synthesized by a 3-hour carbonization time thinly dispersed onto the CFME (Figure 2, left), and modification of the electrode tip is also evident (Figure S1). Surface coverage is relatively low with modification procedures consisting of 700 °C activation heating and this can be attributed to poor electrostatic and pi-pi interactions of the microporous carbon frameworks with CFMEs as compared to previous carbon material modifications.[44–46] The reduced overall surface area of macroporous frameworks compared to lower sized pores reduces pi-pi interactions resulting in electrostatic attractions dominating the interfacial interactions between the carbon fiber and WCG-derived porous carbon. The electrostatic interactions are likely a product of oxide functionality. Micropores generated at lower kinetic parameters play a vital role in these weak interactions as microporous frameworks create greater repulsive surface area interactions across the CFME surface. Meanwhile, modification surface coverage is improved with the porous carbon material synthesized at 900 °C activation heating (Figure 2D) attributed to enhanced kinetic conditions producing macroporous frameworks with less repulsive surface interactions. Although modification surface coverage is improved, there are possible future routes to further address this to improve modification uniformity. Ways to improve this could entail changing the solvent to enhance material solubility, improve material adherence using ion exchange polymers, or dope the material to enhance surface interactions. Of note, gold sputtering was used prior to SEM imaging of modified electrodes due to glass capillary charging. This coating causes obstructed visibility of pores (Figure 2 and Figure S1). WCG-derived porous carbon alone depicts highly visible micro and macroporous distributions.

Pore Size Analysis.—Quantitative pore size analysis of WCG-derived porous carbon was performed using two key pore size/surface area determination techniques: gas physisorption and mercury intrusion porosimetry (MIP). Analysis of mesopore distribution (2 – 150 nm) relied on a volumetric gas adsorption technique in which nitrogen (N_2) adsorbs to the WCG-derived porous carbon surface and the pressure is varied. The condensed gas then fills the material's accessible pores as the relative pressure increases toward saturation allowing pore size distribution quantification correlated to adsorbed volume. When analyzing WCG-derived porous carbon synthesized at 3-hour initial heating, 1:2 WCG:KOH, and 900°C final heating temperature (optimal porous carbon synthesis based on electrochemical characterization), a Brunauer-Emmett-Teller (BET) surface area of 90.30 $m^2\ g^{-1}$ (normalized by sample mass) evident of a highly porous material. Mesopore measurements (Figure 3), best for types II or IV isotherms (Figure 3A) from 2 – 100 nm, used the Barrett, Joyner, and Halenda (BJH) theory to determine specific pore area/diameter of cylindrical equivalent pore volumes. The resulting pore size distribution (Figure 3B) generated by BJH adsorption/desorption gives insight into cumulative pore volumes and average pore diameters. This illustrates a diverse pore diameter distribution with a large population of pores in the size range of ~ 5 – 7 nm and ~ 30.5 nm. This analysis shows a much greater cumulative pore volume at low-nanometer pore dimensions with an average pore diameter of 5.26 nm and volume of 0.03 $cm^3\ g^{-1}$. Pores on this dimensional scale facilitate kinetic improvements to neurotransmitter detection evident upon electrochemical characterization.[13]

MIP is common for macropore analysis where non-wetting mercury intrudes into sample voids as pressure is increased filling larger pores first and smaller pores last to characterize pores from 0.004 – 200 μm in diameter. Of note, MIP analyzes interparticle voids and intraparticle pores, so it can be inferred (coupled with SEM images) that macropores on the large diameter scale for the WCG-derived porous carbon material are interparticle voids while macropores on the low diameter scale are inferred as intraparticle pores. MIP gives information on sample pore area, median pore diameter, and pore diameter distribution. Analysis of the WCG-derived porous carbon synthesized at 3-hour initial heating, 1:2 WCG:KOH, and 900°C final heating shows a total pore area of 17.36 m^2 g^{-1} with 70.9% porosity. The pore diameter distribution (Figure 3C) shows a vast size distribution at low macropore diameters encompassing high overall pore volume quantities. High diameter macropores exhibit a clustered pore volume/diameter region (up to ~ 10 μm) with increasing pore volume as we approach larger pore diameters on the interparticle void regime. Overall, the pore diameter distribution generates a volume based median pore diameter of 26.16 μm greatly impacted by the presence of interparticle voids. The average pore diameter tells a different story, though, where the average pore diameter based on pore intrusion volume is 0.31 μm illustrating a vast network of lower diameter macropores on the dimensional scale possible for local neurotransmitter trapping. A value this low for an average pore diameter implies the population of low-diameter macropores dominates this pore size analysis over the interparticle voids.

Porous carbon modified – CFME electrochemical optimization

The technique to modify the surface of CFMEs is important because it impacts the coverage uniformity, noise, and electrochemical detection. Here, we optimized the modification technique to maximize detection sensitivity while providing minimal impacts to capacitive current. Experiments to test the extent to which the electrode modification technique impacted electrochemical detection of dopamine used WCG-derived porous carbon synthesized at a 700 ° initial heating for 2-hours, 2:1 WCG:KOH mixing ratio, and 700 °C final heating for 2-hours (Figure 4A). Drop casting, dip coating, and electrodeposition were tested as potential modification techniques and all solutions were prepared in 2 mg/mL porous carbon/H_2O (Figure 4A). Electrodes were pretested using 1 μM dopamine at the traditional FSCV waveform (See Methods).

Macroporous frameworks developed by WCGs have more attractive surface chemistry consisting of higher defect degrees and edge plane character for improved dopamine interfacial interactions while also permitting momentary trapping for short-term dopamine cyclization. These porous carbon properties assist dopamine redox species' adsorption for improved FSCV detection. Dopamine's peak oxidative current was analyzed prior to modification (i_{pre}) and compared to the post-modified electrode (i_{post}): the ratio of these two currents were plotted as a function of electrode modification technique (Figure 4A). An i_{post}/i_{pre} ratio above 1.0 indicates increased oxidative current denoting modification improvements. Overall, we demonstrate significant improvements using dip coating with a 1.4 ± 0.2 - fold increase in oxidative current for dopamine (One-way ANOVA, Bonferroni posttest, $p = 0.05$, $n=15$). Little to no improvements were observed for drop casting and electrodeposition while decreasing S/N attributed to poor distribution of porous carbon

across the CFME/s surface. Therefore, we chose dip coating as the optimal modification technique. Although we observed a significant improvement in oxidative current, the overall change was not large so separate experiments (described below) optimizing the material synthesis were done to improve overall oxidative current increases.

Carbonization time, WCG:KOH ratio, and annealing temperature were separately optimized and shown to significantly impact dopamine electrochemical detection. The initial synthetic route, as described above, included heating at 700°C for 2 hours, a 2:1 WCG:KOH, and annealing at 700°C for 2-hours. First, we compared the extent to which the initial heating time impacts detection by comparing 3 hours to 2 hours while keeping the rest of the synthetic route unchanged (Figure 4B). We show that by extending the initial heating time to 3-hours i_{post}/i_{pre} enhancements are improved from 1.4 ± 0.2 to 2.3 ± 0.1. We speculate that the extended heating time ensures full expulsion of all contaminants from the carbonized coffee grounds.

Second, we tested the extent to which the weight ratio of WCG and KOH impacts detection. For this experiment, the synthetic route included the optimized 3 hour carbonization heating and annealing at 700°C for 2 hours while the WCG;KOH was altered from 2:1 to 1:2. We hypothesized that increasing KOH abundance would provide extended activation to increase carbon lattice pore abundance and size While calculating oxidative current enhancements while using 1:2 WCG:KOH, we note no statistical increase in the i_{post}/i_{pre} (2.6 ± 0.2, unpaired t-test, $p = 0.23$, n=15). Although oxidative current improvements remained on par with 2:1 WCG:KOH, 1:2 WCG:KOH synthesis increased pore quantity due to a higher KOH composition allowing for a greater extent of activation. We speculate that this is due to larger pore networks on the surface enabling local trapping.[17,22]

Finally, the extent to which the annealing temperature impacts electrochemical detection was investigated (Figure 4D). In these experiments, the optimal carbonization time (3-hours at 700°C) and WCG:KOH ratio (1:2) were used, while varying annealing temperature from 700 to 900 °C. Previous reports note that increasing the annealing temperature above 700°C elicits additional activation mechanisms enabling sub-nanometer pore formation.[5,6,10] In theory, a higher annealing temperature should form extensive nanopore networks creating higher-ordered nanopores. We observed a significant increase in the oxidative current annealing at 900 °C (Figure 4D, 3.5 ± 0.4, unpaired t-test, $p = 0.03$, n=15). Overall, we provide evidence that pore uniformity and size significantly impact electrochemical detection with negligible impacts to temporal resolution and electrode stability (Figure 4, S4, S5,and Table 1).

The optimal synthetic route for making WCG porous carbon material includes an initial heating time of 3 hours, a 2:1 ratio of WCG to KOH, and a final annealing temperature of 900 °C. WCG porous carbon not only improved oxidative current, but also significantly improves dopamine's interfacial interactions. Further electrochemical characterization reveals impacts to electrochemical reversibility. Figure 5 shows an example cyclic voltammogram (CV) for 1 μM dopamine and the background charging current before and after dip-coating. Electrochemical reversibility is calculated by taking the ratio of the oxidation current to the reduction current (i_{ox}/i_{red}): a ratio of 1.0 indicates

perfect reversibility. Electrochemical reversibility was compared prior to and after electrode modification. Overall, the WCG-modified CFMEs significantly enhanced electrochemical reversibility from 2.2 ± 0.1 (bare) to 1.9 ± 0.1 (modified) (Figure S6, Table 2, paired t-test, p = 0.05, n=15). Lower electrochemical reversibility is observed on bare CFMEs because it is known that dopamine adsorbs 10x more strongly than dopamine-*o*-quinone (DOQ, Figure 5A and C black trace) resulting in diffusional loss of DOQ.[47] CVs at modified electrode surfaces show higher reduction currents indicating improved electrochemical reversibility. This data supports prior work that suggests porous and roughened surfaces promote enhanced dopamine interfacial interactions.[13,16,17,20,22] As expected, we observe small increases in non-faradaic capacitive current following dip coating from 1980 ± 210 nA to 2260 ± 210 nA (Figure 5D and Table 2, paired t-test, p = 0.027, n=15). This is likely attributed to the larger surface area of the synthesized porous carbon and small increases in noise caused by the non-uniformity of the surface modification (Figure 2D). We observed similar results in prior work modifying the surface with porous carbon nanofibers.[13]

Sensitivity, Limit of Detection, and Frequency Dependence

CFME modifications with optimally synthesized WCG-derived porous carbon provides a 2-fold increase in dopamine detection sensitivity. For analysis, concentrations were tested ranging from 500 nM to 300 μM on bare and WCG-derived porous carbon modified CFMEs to determine sensitivity and LOD (Figure 6, n = 6). The traditional linear working region extends to 10 μM and was therefore used for this analysis (Figure 6A). The sensitivity increased from 9.8 ± 0.5 nA/μM (R^2 = 0.92) for bare to 20.6 ± 1.6 nA/μM (R^2 = 0.80) for porous carbon modified CFMEs (Table 2, Figure 6A). We speculate the 2.1-fold increase in sensitivity is attributed to increased adsorption sites added to the surface. We note a low linearity coefficient for porous carbon modified CFMEs attributed to hindered modification reproducibility due to poor pi-pi interactions limiting surface coverage following modification. The LOD was determined as three multiplied by the standard deviation of the noise. We report an improvement in the LOD at porous carbon modified CFMEs from 13.7 ± 5.0 nM to 5.3 ± 2.0 nM (Table 2, unpaired t-test, p = 0.15, n = 6). Bare CFMEs begin to saturate at concentrations greater than 10 μM (Figure 6B, black); whereas the current does not appear to saturate as dramatically in this same regime for WCG-modified electrodes (Figure 6B, orange). We propose an increase in interaction sites at the modified surfaces result in less surface saturation. These enhancements to the electrode's surface offer a direction to addressing low sensitivity of other neurochemicals detected using FSCV.

Surveying different neurochemical structures/classes is important for understanding the impact these novel materials have on sensing beyond dopamine by performing similar analyses (i_{post}/i_{pre}, Figure S7). At CFMEs, norepinephrine, despite its nearly identical structure to dopamine, exhibits much lower detection sensitivity than dopamine, but WCG modifications enhanced oxidation current 2.1 ± 0.3 – fold (Figure S7 A) with slightly slowed electron transfer rates. Similarly, the purines guanosine and adenosine (Figures S7 B-C) show primary oxidation current improvements of 2.3 ± 0.3 and 1.2 ± 0.1 – fold respectively illustrating the unique surface interactions of similar neurochemical structures vastly differing in their detection enhancements. Adenosine has been shown to interact

more poorly at edge plane-enhanced electrodes indicating that WCG-derived porous carbon modifications could hinder adenosine detection improvements.[48] Additional neurochemical structures, ascorbic acid, serotonin, and histamine (Figure S7D-F), exhibited slowed electron transfer rates with increases in oxidation current of 2.4 ± 0.4, 1.9 ± 0.2, and 1.4 ± 0.1 – fold respectively. Overall, WCG-modified CFMEs present a viable electrode material for enhanced FSCV detection utility for numerous other neurochemicals with slightly sluggish electron transfer kinetics.

WCG-derived porous carbon material reduces the impact of increasing waveform application frequency on measured oxidative current compared to traditional CFMEs. Previous reports have demonstrated that porous electrode geometries result in frequency independent behavior with FSCV.[18,22] The traditional waveform application frequency with FSCV is 10 Hz leading to a 100 millisecond time between scans. Increasing the waveform application frequency, while maintaining other waveform parameters, results in a decrease in preconcentration time between scans. Bare CFMEs exhibit detrimental loss in oxidative current as a function of increasing application frequency, but WCG-derived porous carbon provides improved electrochemical reversibility which we hypothesize creates less frequency dependent measurements. Here, we show WCG-derived porous material significantly impacts the loss of oxidative current observed at high frequencies (Figure 7). The applied frequency was increased from 10 Hz up to 100 Hz (Figure 7) reducing dopamine adsorption time from 91.5 ms to 1.5 ms. Oxidative current was normalized to the current observed at 10 Hz to determine the relative loss in current as a function of frequency. We observed small improvements in the calculated loss of oxidative current for dopamine at 100 Hz improving from 83.20 ± 0.04 % for bare CFME to 63.62 ± 0.07% for the modified electrodes (Figure S9, unpaired t-test, $p = 0.032$, $n=6$, Table 2). Although we did not achieve complete frequency independent behavior compared to prior reports at carbon nanomaterials,[18,22] we can attribute this to the lack of uniform coating of the WCG-derived porous material on the surface. In the future, electrodes of entirely WCG-derived porous material would provide the field of biosensing an environmentally friendly approach to fabricating biosensors with significantly improved temporal resolution capabilities. Although the use of biomass in this work is environmentally friendly, we acknowledge the overall environmental impact of our work alone is low due to low amounts of WCG used. Hopefully this work sparks biomass utility in other biosensor applications where we begin to see large- scale applications.

Catecholamine detection validation in mesenteric lymph node with WCG-modified CFMEs

Mesenteric lymph nodes (MLN), located within the mesentery of the intestines, play a crucial role in facilitating rapid immune response to gut infections. Sympathetic neurons innervate MLNs and release norepinephrine (NE) to communicate with immune cells, directing immune cell response.[49] Understanding the dynamics of NE neuronal release is a crucial area of importance for studying the gut-brain-immune axis.[50]. Due to the enhanced sensitivity of WCG-derived porous carbon modified CFMEs, they were tested in MLN slices to validate neurotransmitter detection in a biological matrix to demonstrate practical applicability. Electrodes were implanted 100 μM away from a glass capillary that exogenously applied a picoliter drop of 25 μM DA (Figure 8A-C) or 25 μM NE (Figure

8D-F). The higher concentration of analytes was necessary as the analytes need to diffuse through the tissue before being detectable by the electrode similar to prior reports.[51,52] The current versus time plot for DA (Figure 8A) and NE (Figure 8D) show rapid detection after the analyte application at 15 seconds and then the drop off in current due to the analyte diffusing away or cell reuptake. For both analytes, there is a peak shift to 0.7 V; this is larger than what was observed in the flow cell for WCG-modified CFMEs. The peak shift is likely a matrix effect and is clearly observed in the CV for DA (Figure 8C) and NE (Figure 8F). Minor changes are observed in DA versus NE peak shape, likely due to varying tissue slices for each analyte. Other differences, such as current magnitude, could be due to the distance between the glass capillary electrode and the WCG-modified CFMEs. Overall, this demonstrates the practicality of using WCG-modified CFMEs in biological studies.

Conclusion

The carbonization of biowastes has long been used for battery and energy storage applications, but we report an optimized method for re-purposing these eco-friendly materials to enhance neurochemical detection using FSCV. Dip coating of WCG-derived porous carbon onto CFMEs provides improvements in the quantity of adsorption sites available for dopamine redox interactions. These improvements, with minimal capacitive current increases, supply enhancements in dopamine detection sensitivity, limits of detection, and electrochemical reversibility for decreased frequency dependence. We hypothesize that these enhancements directly correlate to local trapping of dopamine stemming from the hierarchical pore networks produced by carbonaceous biowaste activation. These modified electrodes also show utility for enhanced detection of neurochemicals other than dopamine while showing viability of detection in the mesenteric lymph node for stimulated norepinephrine detection. Overall, dip coating of WCG-derived porous carbon onto CFMEs highlights the first application of re-purposed coffee biowastes for biological electrochemical sensing.

Supplementary Material

Refer to Web version on PubMed Central for supplementary material.

Acknowledgements

The research reported in this manuscript was supported by the National Institute of Allergy and Infection Diseases of the National Institutes of Health under Award Number R01AI151552, the National Science Foundation under Award Number 2143520, and the Alfred P. Sloan Foundation (Grant #FG-2022–18400). The content is solely the responsibility of the authors and does not necessarily represent the official views of the NIH, NSF, or Alfred P. Sloan Foundation. The researchers would also like to thank the NSF REU (CH-1950244) Program for supporting Kamya Lapsley on this project.

References

(1). L, W.; X, H. Recent Advances in Porous Carbon Materials for Electrochemical Energy Storage. Chem Asian J 2018, 13 (12), 1518–1529. 10.1002/asia.201800553. [PubMed: 29667345]

(2). Tang Y; Liu Z; Zhao K Fabrication of Hollow and Porous Polystyrene Fibrous Membranes by Electrospinning Combined with Freeze-Drying for Oil Removal from Water. Journal of Applied Polymer Science 2019, 136 (13), 47262. 10.1002/app.47262.

(3). Brahma S; Ramanujam K; Gardas RL Nitrogen-Doped High Surface Area Porous Carbon Material Derived from Biomass and Ionic Liquid for High-Performance Supercapacitors. Ind. Eng. Chem. Res 2022. 10.1021/acs.iecr.2c00195.

(4). Mukherjee A; Okolie JA; Niu C; Dalai AK Experimental and Modeling Studies of Torrefaction of Spent Coffee Grounds and Coffee Husk: Effects on Surface Chemistry and Carbon Dioxide Capture Performance. ACS Omega 2022, 7 (1), 638–653. 10.1021/acsomega.1c05270. [PubMed: 35036730]

(5). Romanos J; Beckner M; Rash T; Firlej L; Kuchta B; Yu P; Suppes G; Wexler C; Pfeifer P Nanospace Engineering of KOH Activated Carbon. Nanotechnology 2012, 23 (1), 015401. 10.1088/0957-4484/23/1/015401. [PubMed: 22156024]

(6). Chung DY; Son YJ; Yoo JM; Kang JS; Ahn C-Y; Park S; Sung Y-E Coffee Waste-Derived Hierarchical Porous Carbon as a Highly Active and Durable Electrocatalyst for Electrochemical Energy Applications. ACS Appl. Mater. Interfaces 2017, 9 (47), 41303–41313. 10.1021/acsami.7b13799. [PubMed: 29094595]

(7). Li Y; Lu C; Zhang S; Su F-Y; Shen W; Zhou P; Ma C Nitrogen- and Oxygen-Enriched 3D Hierarchical Porous Carbon Fibers: Synthesis and Superior Supercapacity. Journal of Materials Chemistry A 2015, 3 (28), 14817–14825. 10.1039/C5TA02702K.

(8). Yan C; Meng N; Lyu W; Li Y; Wang L; Liao Y Hierarchical Porous Hollow Carbon Spheres Derived from Spirofluorene- and Aniline-Linked Conjugated Microporous Polymer for Phase Change Energy Storage. Carbon 2021, 176, 178–187. 10.1016/j.carbon.2020.12.035.

(9). Zhou Z; Liu T; Khan AU; Liu G Block Copolymer–Based Porous Carbon Fibers. Science Advances 2019, 5 (2), eaau6852. 10.1126/sciadv.aau6852. [PubMed: 30746487]

(10). Zhao P; Shiraz MHA; Zhu H; Liu Y; Tao L; Liu J Hierarchically Porous Carbon from Waste Coffee Grounds for High-Performance Li–Se Batteries. Electrochimica Acta 2019, 325, 134931. 10.1016/j.electacta.2019.134931.

(11). Liu X; Zhang S; Wen X; Chen X; Wen Y; Shi X; Mijowska E High Yield Conversion of Biowaste Coffee Grounds into Hierarchical Porous Carbon for Superior Capacitive Energy Storage. Sci Rep 2020, 10 (1), 3518. 10.1038/s41598-020-60625-y. [PubMed: 32103118]

(12). Liu L; Liu L; Wang Y; Ye B-C A Novel Electrochemical Sensor Based on Bimetallic Metal–Organic Framework-Derived Porous Carbon for Detection of Uric Acid. Talanta 2019, 199, 478–484. 10.1016/j.talanta.2019.03.008. [PubMed: 30952287]

(13). Ostertag BJ; Cryan MT; Serrano JM; Liu G; Ross AE Porous Carbon Nanofiber-Modified Carbon Fiber Microelectrodes for Dopamine Detection. ACS Appl. Nano Mater 2022, 5 (2), 2241–2249. 10.1021/acsanm.1c03933. [PubMed: 36203493]

(14). Li Y; Ross AE Plasma-Treated Carbon-Fiber Microelectrodes for Improved Purine Detection with Fast-Scan Cyclic Voltammetry. Analyst 2020, 145 (3), 805–815. 10.1039/C9AN01636H. [PubMed: 31820742]

(15). Vreeland RF; Atcherley CW; Russell WS; Xie JY; Lu D; Laude ND; Porreca F; Heien ML Biocompatible PEDOT:Nafion Composite Electrode Coatings for Selective Detection of Neurotransmitters in Vivo. Anal. Chem 2015, 87 (5), 2600–2607. 10.1021/ac502165f. [PubMed: 25692657]

(16). Cao Q; Hensley DK; Lavrik NV; Venton BJ Carbon Nanospikes Have Better Electrochemical Properties than Carbon Nanotubes Due to Greater Surface Roughness and Defect Sites. Carbon 2019, 155, 250–257. 10.1016/j.carbon.2019.08.064. [PubMed: 31588146]

(17). Shao Z; Puthongkham P; Hu K; Jia R; Mirkin MV; Venton BJ Thin Layer Cell Behavior of CNT Yarn and Cavity Carbon Nanopipette Electrodes: Effect on Catecholamine Detection. Electrochimica Acta 2020, 361, 137032. 10.1016/j.electacta.2020.137032. [PubMed: 32981947]

(18). Cao Q; Shao Z; Hensley DK; Lavrik NV; Venton BJ Influence of Geometry on Thin Layer and Diffusion Processes at Carbon Electrodes. Langmuir 2021, 37 (8), 2667–2676. 10.1021/acs.langmuir.0c03315. [PubMed: 33591763]

(19). Mendoza A; Asrat T; Liu F; Wonnenberg P; Zestos AG Carbon Nanotube Yarn Microelectrodes Promote High Temporal Measurements of Serotonin Using Fast Scan Cyclic Voltammetry. Sensors (Basel) 2020, 20 (4), 1173. 10.3390/s20041173. [PubMed: 32093345]

(20). Zestos AG; Yang C; Jacobs CB; Hensley D; Venton BJ Carbon Nanospikes Grown on Metal Wires as Microelectrode Sensors for Dopamine. Analyst 2015, 140 (21), 7283–7292. 10.1039/C5AN01467K. [PubMed: 26389138]

(21). Puthongkham P; Yang C; Venton BJ Carbon Nanohorn-Modified Carbon Fiber Microelectrodes for Dopamine Detection. Electroanalysis 2018, 30 (6), 1073–1081. 10.1002/elan.201700667. [PubMed: 30613128]

(22). Yang C; Hu K; Wang D; Zubi Y; Lee ST; Puthongkham P; Mirkin MV; Venton BJ Cavity Carbon-Nanopipette Electrodes for Dopamine Detection. Anal. Chem 2019, 91 (7), 4618–4624. 10.1021/acs.analchem.8b05885. [PubMed: 30810304]

(23). Weese ME; Krevh RA; Li Y; Alvarez NT; Ross AE Defect Sites Modulate Fouling Resistance on Carbon-Nanotube Fiber Electrodes. ACS Sens 2019, 4 (4), 1001–1007. 10.1021/acssensors.9b00161. [PubMed: 30920207]

(24). Harreither W; Trouillon R; Poulin P; Neri W; Ewing AG; Safina G Carbon Nanotube Fiber Microelectrodes Show a Higher Resistance to Dopamine Fouling. Anal. Chem 2013, 85 (15), 7447–7453. 10.1021/ac401399s. [PubMed: 23789970]

(25). Yang C; Wang Y; Jacobs CB; Ivanov IN; Venton BJ O2 Plasma Etching and Antistatic Gun Surface Modifications for CNT Yarn Microelectrode Improve Sensitivity and Antifouling Properties. Anal. Chem 2017, 89 (10), 5605–5611. 10.1021/acs.analchem.7b00785. [PubMed: 28423892]

(26). Lee J; Jeong S; Ye Y; Chen V; Vigneswaran S; Leiknes T; Liu Z Protein Fouling in Carbon Nanotubes Enhanced Ultrafiltration Membrane: Fouling Mechanism as a Function of pH and Ionic Strength. Separation and Purification Technology 2017, 176, 323–334. 10.1016/j.seppur.2016.10.061.

(27). Ostertag B; Ross AE Wet-Spun Porous Carbon Microfibers for Enhanced Electrochemical Detection. ACS Appl. Mater. Interfaces 2023, 15 (14), 17601–17611. 10.1021/acsami.3c00423. [PubMed: 36989172]

(28). Yun YS; Park MH; Hong SJ; Lee ME; Park YW; Jin H-J Hierarchically Porous Carbon Nanosheets from Waste Coffee Grounds for Supercapacitors. ACS Appl. Mater. Interfaces 2015, 7 (6), 3684–3690. 10.1021/am5081919. [PubMed: 25612009]

(29). Xiao C; Wang S; Guo Y; Zhang Y; Hasi Q-M; Tian Q; Chen L Coffee Grounds-Doped Alginate Porous Materials for Efficient Solar Steam Generation. Langmuir 2022, 38 (5), 1888–1896. 10.1021/acs.langmuir.1c03102. [PubMed: 35080896]

(30). Xu H; Xie L; Hakkarainen M Coffee-Ground-Derived Quantum Dots for Aqueous Processable Nanoporous Graphene Membranes. ACS Sustainable Chem. Eng 2017, 5 (6), 5360–5367. 10.1021/acssuschemeng.7b00663.

(31). Kim DJ; Yoo JM; Suh Y; Kim D; Kang I; Moon J; Park M; Kim J; Kang K-S; Hong BH Graphene Quantum Dots from Carbonized Coffee Bean Wastes for Biomedical Applications. Nanomaterials (Basel) 2021, 11 (6), 1423. 10.3390/nano11061423. [PubMed: 34071339]

(32). Gupta N; Sen K; Singh V; Soni A; Kapoor M Electrochemical Sensing of Dopamine Using Graphene Oxide Derived from Pine Needle Bio-Waste. AIP Conference Proceedings 2020, 2265 (1), 030079. 10.1063/5.0025334.

(33). Shin D; Choun M; Chul Ham H; Kwang Lee J; Lee J A Graphitic Edge Plane Rich Meso-Porous Carbon Anode for Alkaline Water Electrolysis. Physical Chemistry Chemical Physics 2017, 19 (33), 21987–21995. 10.1039/C7CP03208K. [PubMed: 28808708]

(34). Pour N; Kwabi DG; Carney T; Darling RM; Perry ML; Shao-Horn Y Influence of Edge- and Basal-Plane Sites on the Vanadium Redox Kinetics for Flow Batteries. J. Phys. Chem. C 2015, 119 (10), 5311–5318. 10.1021/jp5116806.

(35). Kneten KR; McCreery RL Effects of Redox System Structure on Electron-Transfer Kinetics at Ordered Graphite and Glassy Carbon Electrodes. Anal. Chem 1992, 64 (21), 2518–2524. 10.1021/ac00045a011.

(36). Ferrari AC; Basko DM Raman Spectroscopy as a Versatile Tool for Studying the Properties of Graphene. Nature Nanotech 2013, 8 (4), 235–246. 10.1038/nnano.2013.46.

(37). Wu J-B; Lin M-L; Cong X; Liu H-N; Tan P-H Raman Spectroscopy of Graphene-Based Materials and Its Applications in Related Devices. Chemical Society Reviews 2018, 47 (5), 1822–1873. 10.1039/C6CS00915H. [PubMed: 29368764]

(38). Dresselhaus MS; Jorio A; Saito R Characterizing Graphene, Graphite, and Carbon Nanotubes by Raman Spectroscopy. Annual Review of Condensed Matter Physics 2010, 1 (1), 89–108. 10.1146/annurev-conmatphys-070909-103919.

(39). Li Y; Fleischer M, C.; Ross E, A. High Young's Modulus Carbon Fibers Are Fouling Resistant with Fast-Scan Cyclic Voltammetry. Chemical Communications 2020, 56 (58), 8023–8026. 10.1039/D0CC02517H. [PubMed: 32453308]

(40). Syeed AJ; Li Y; Ostertag BJ; Brown JW; Ross AE Nanostructured Carbon-Fiber Surfaces for Improved Neurochemical Detection. Faraday Discuss 2021. 10.1039/D1FD00049G.

(41). Claramunt S; Varea A; López-Díaz D; Velázquez MM; Cornet A; Cirera A The Importance of Interbands on the Interpretation of the Raman Spectrum of Graphene Oxide. J. Phys. Chem. C 2015, 119 (18), 10123–10129. 10.1021/acs.jpcc.5b01590.

(42). King AAK; Davies BR; Noorbehesht N; Newman P; Church TL; Harris AT; Razal JM; Minett AI A New Raman Metric for the Characterisation of Graphene Oxide and Its Derivatives. Sci Rep 2016, 6 (1), 19491. 10.1038/srep19491. [PubMed: 26775647]

(43). Cao Q; Puthongkham P; Venton BJ Review: New Insights into Optimizing Chemical and 3D Surface Structures of Carbon Electrodes for Neurotransmitter Detection. Anal Methods 2019, 11 (3), 247–261. 10.1039/C8AY02472C. [PubMed: 30740148]

(44). Hočevar SB; Wang J; Deo RP; Musameh M; Ogorevc B Carbon Nanotube Modified Microelectrode for Enhanced Voltammetric Detection of Dopamine in the Presence of Ascorbate. Electroanalysis 2005, 17 (5–6), 417–422. 10.1002/elan.200403175.

(45). Chang Y; Venton BJ Optimization of Graphene Oxide-Modified Carbon-Fiber Microelectrode for Dopamine Detection. Anal Methods 2020, 12 (22), 2893–2902. 10.1039/d0ay00310g. [PubMed: 32617123]

(46). Taylor IM; Robbins EM; Catt KA; Cody PA; Weaver CL; Cui XT Enhanced Dopamine Detection Sensitivity by PEDOT/Graphene Oxide Coating on in Vivo Carbon Fiber Electrodes. Biosens Bioelectron 2017, 89 (Pt 1), 400–410. 10.1016/j.bios.2016.05.084. [PubMed: 27268013]

(47). Venton BJ; Cao Q Fundamentals of Fast-Scan Cyclic Voltammetry for Dopamine Detection. Analyst 2020, 145 (4), 1158–1168. 10.1039/C9AN01586H. [PubMed: 31922176]

(48). Jarosova R; Ostertag J, B.; Ross E, A. Graphene Oxide Fiber Microelectrodes with Controlled Sheet Alignment for Sensitive Neurotransmitter Detection. Nanoscale 2023. 10.1039/D3NR02879H.

(49). Murray K; Barboza M; Rude KM; Brust-Mascher I; Reardon C Functional Circuitry of Neuro-Immune Communication in the Mesenteric Lymph Node and Spleen. Brain Behav Immun 2019, 82, 214–223. 10.1016/j.bbi.2019.08.188. [PubMed: 31445965]

(50). Jacobson A; Yang D; Vella M; Chiu IM The Intestinal Neuro-Immune Axis: Crosstalk between Neurons, Immune Cells, and Microbes. Mucosal Immunol 2021, 14 (3), 555–565. 10.1038/s41385-020-00368-1. [PubMed: 33542493]

(51). Hensley AL; Colley AR; Ross AE Real-Time Detection of Melatonin Using Fast-Scan Cyclic Voltammetry. Anal. Chem 2018, 90 (14), 8642–8650. 10.1021/acs.analchem.8b01976. [PubMed: 29932641]

(52). Cryan MT; Ross AE Scalene Waveform for Codetection of Guanosine and Adenosine Using Fast-Scan Cyclic Voltammetry. Anal. Chem 2019, 91 (9), 5987–5993. 10.1021/acs.analchem.9b00450. [PubMed: 30938508]

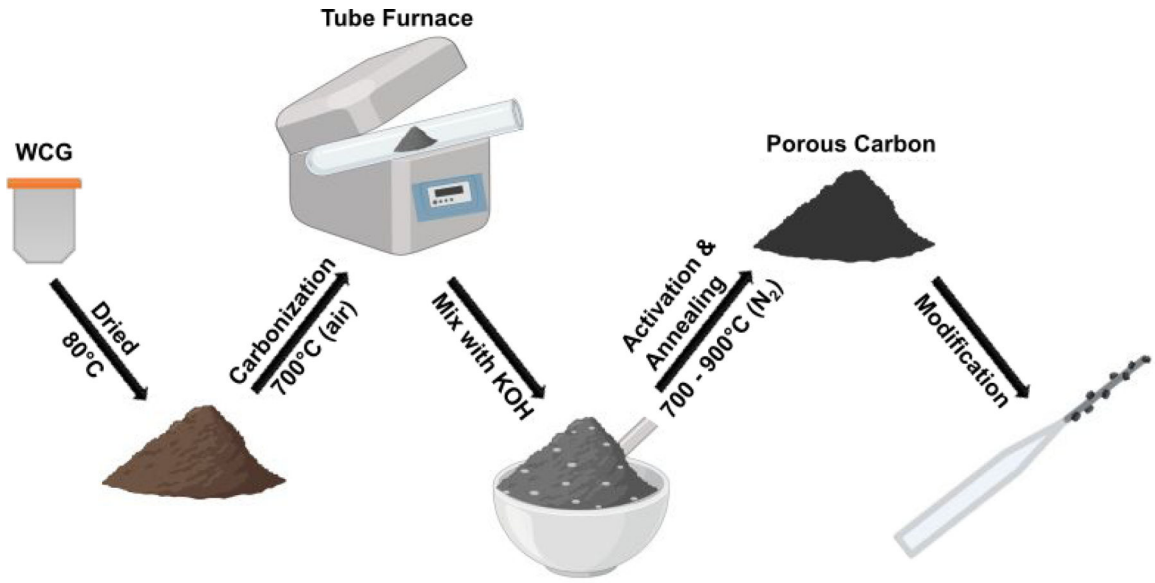

Figure 1:
Schematic of WCG-derived nanoporous carbon synthesis and application. The synthesis involves drying and carbonizing WCG's at high temperatures to remove contaminants followed by mixing with KOH and a final heating step for chemical activation and pyrolysis. Once the material is synthesized, it is used to modify CFMEs (Created with BioRender.com).

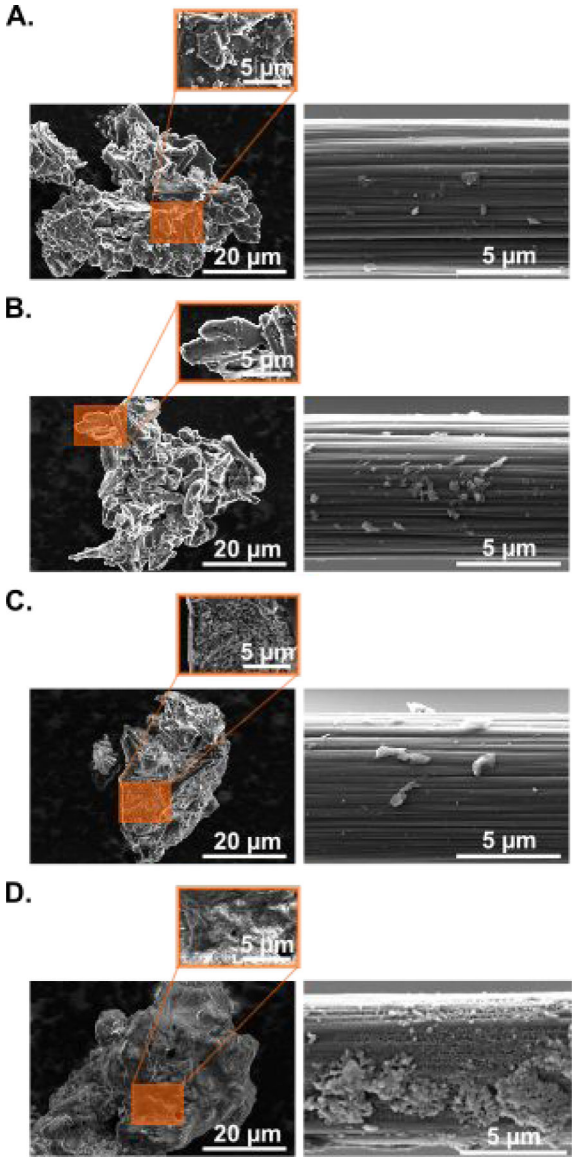

Figure 2:

Changing the carbonization time, ratio of WCG and KOH, and activation heating temperature impacts pore abundance and surface coverage of CFME following dip-coating modification (right). A) WCG initially heated at 700°C for 2 hours in air, 2:1 WCG:KOH, and a final heating of 700°C for 2 hours in N_2. (B) WCG initially heated at 700°C for 3 hours in air, 2:1 WCG:KOH, and a final heating of 700°C for 2 hours in N_2. (C) WCG initially heated at 700°C for 3 hours in air, 1:2 WCG:KOH, and a final heating of 700°C for 2 hours in N_2. (D) WCG initially heated at 700°C for 3 hours in air, 1:2 WCG:KOH, and a final heating of 900°C for 2 hours in N_2. Scale bar shown on images.

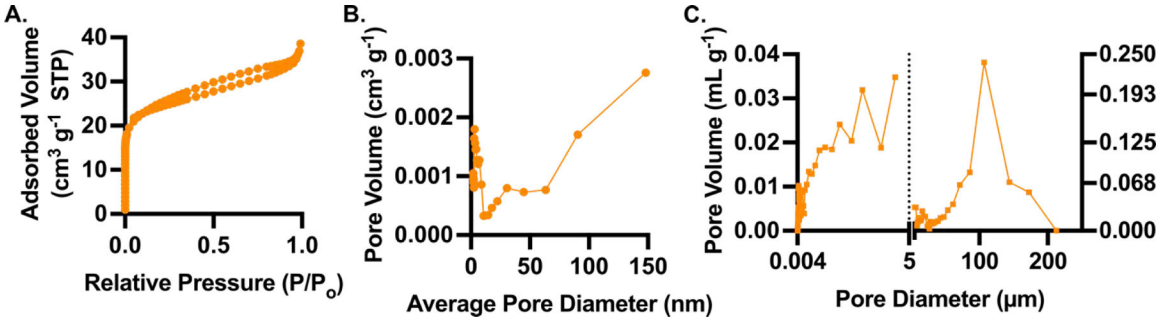

Figure 3:

N_2 physisorption isotherm accompanied by mercury intrusion porosimetry illustrate a mesopore (2 – 150 nm) and macropore (0.004 – 200μm) WCG-derived porous carbon framework with varying pore width distribution regimes. (A) N_2 physisorption isotherm with (B) corresponding mesopore volume versus pore diameter. (C) Mercury intrusion porosimetry analysis of macropores from 0.004 – 5.000 μm (left) and 5 – 200 μm (right).

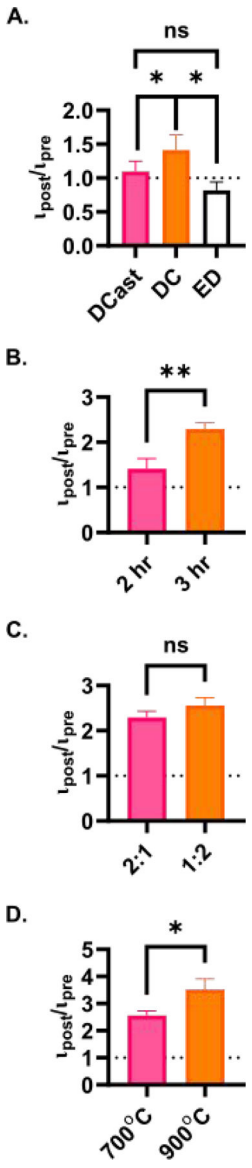

Figure 4:

The WCG-derived nanoporous carbon synthesis steps and method of electrode modification directly impact the electrochemical detection of dopamine. A) The electrode modification procedure was tested using the initial synthetic route (2 hr initial heating, 1:2 WCG: KOH, and 700 °C annealing temperature). The procedures compared include drop casting, dip coating, and electrodeposition. Dip coating produced the highest improvement in oxidative current for 1 μM dopamine with FSCV and was used for all other optimization steps (One-way ANOVA, Bonferroni posttest, $p = 0.05$, $n = 15$). (B) A 2- and 3-hour initial heating temperature of WCG's was compared and longer initial heating significantly improved dopamine detection (Unpaired t-test, $p = 0.003$, $n=15$). (C) Changing the WCG: KOH ratio from 2:1 and 1:2 did not significantly influence dopamine detection (Unpaired t-test, $p = 0.23$, $n = 15$). (D) The annealing temperature significantly impacted the observed improvement in dopamine detection (Unpaired t-test, $p = 0.03$, $n = 15$).

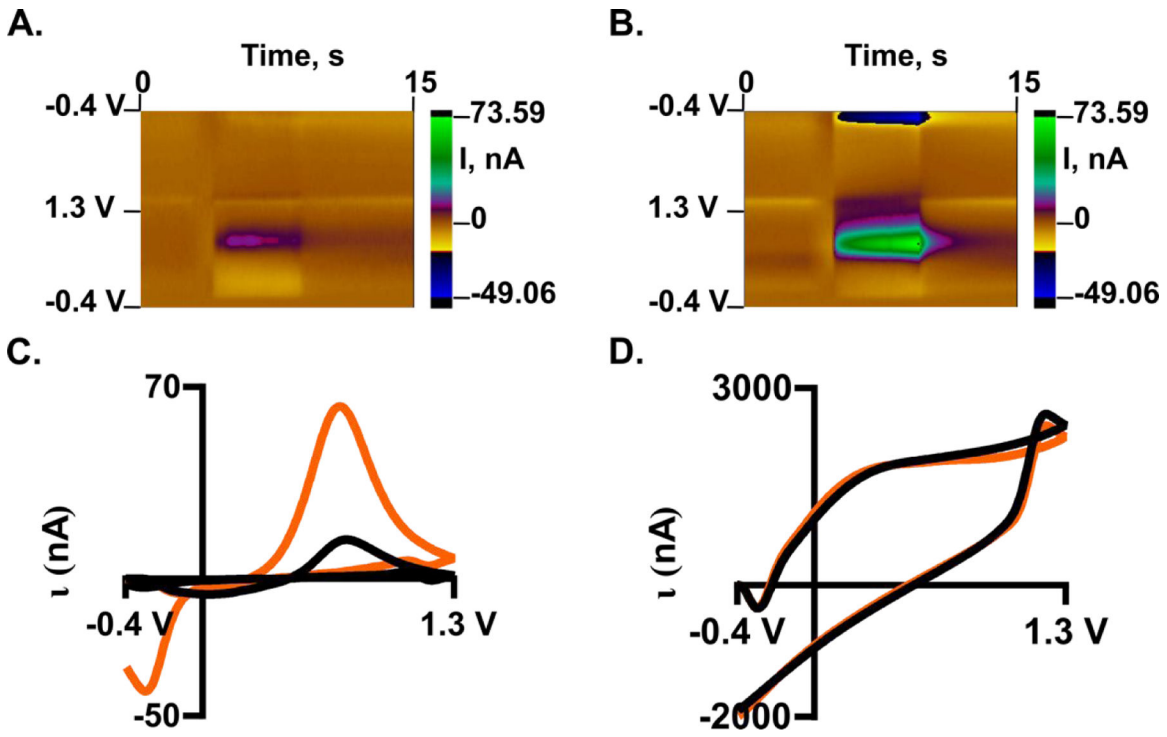

Figure 5:

CFMEs modified with WCG-derived nanoporous carbon (3-hour initial heating, 1:2 WCG:KOH, and 900C final heating) show significant enhancements in faradaic current and redox cycling for 1 μM DA with small changes in non-faradaic current. Example false color plots of a (A) bare CFME and (B) WCG-derived nanoporous carbon modified CFME after dip coating. Corresponding background-subtracted (C) and background (D) CVs for bare (black) and modified (orange) CFME (n=15).

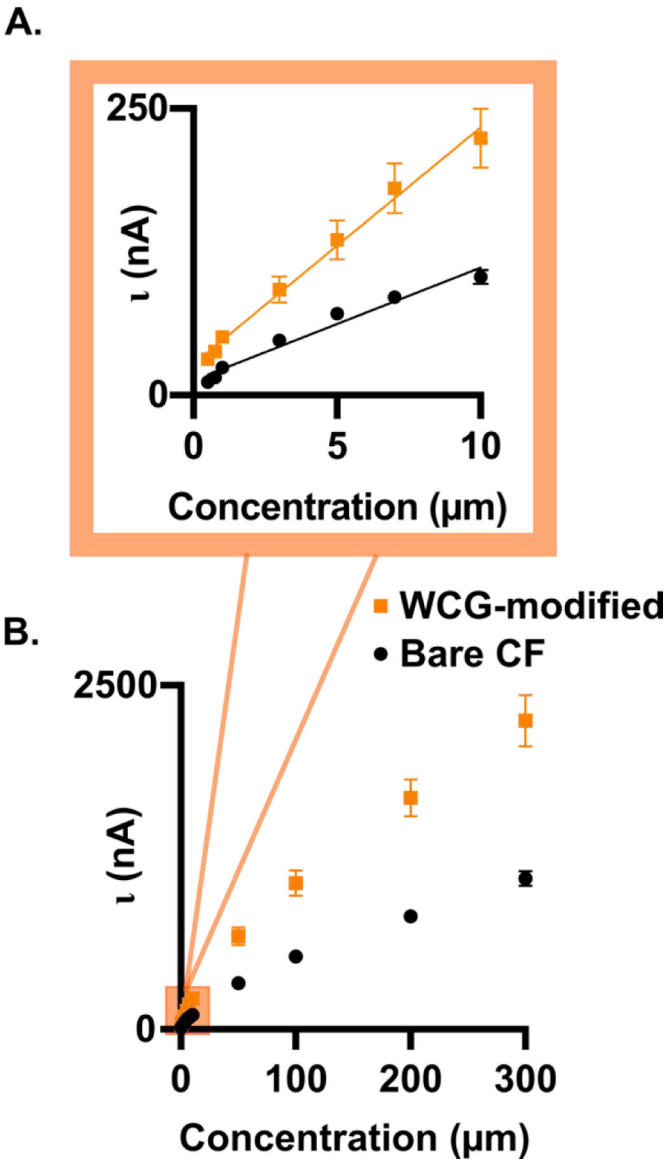

Figure 6:

Waste coffee ground – derived porous carbon (3-hour initial heating, 1:2 WCG:KOH, and 900C final heating) provides enhanced detection sensitivity to dopamine (n = 6). (A) The dynamic range (linear region, 500 nM to 10 μM) for dopamine was used to calculate the sensitivity of measurement. The slope of the linear calibration curve changed from 9.8 ± 0.5 nA/μM (bare CFME, R^2 = 0.92) to 20.6 ± 1.6 nA/μM (WCG-modified CFME, R^2 = 0.80). (B) Concentrations from 500 nM to 300 μM were tested for bare and porous carbon modified – CFMEs to demonstrate the differences in saturation point at the surface.

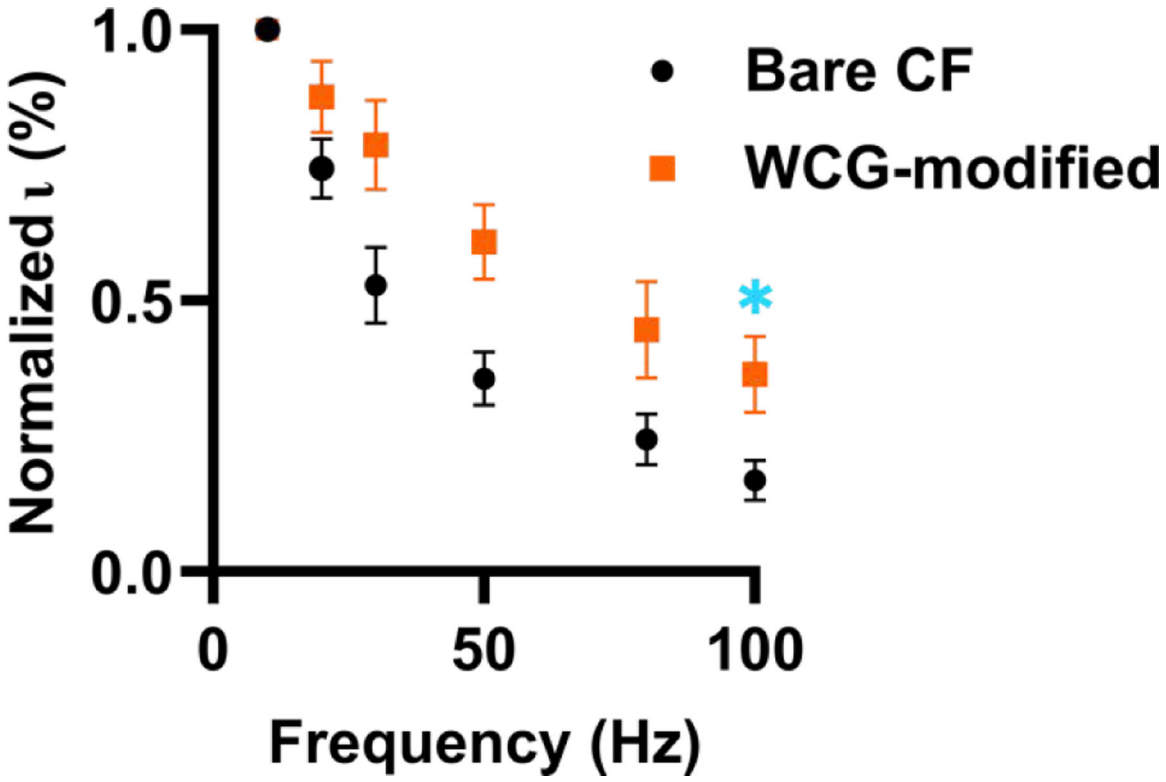

Figure 7:

Significant improvement in observed percent loss of oxidative current for dopamine is demonstrated at WCG-derived porous carbon-modified electrodes (3-hour initial heating, 1:2 WCG:KOH, and 900C final heating). Oxidative current for dopamine was normalized to the current observed at 10 Hz for both the bare and modified electrodes. The waveform used scanned from −0.4 to 1.3 V at 400 V/s. A significant improvement was observed at the 100 Hz waveform application frequency indicating that there is less loss in oxidative current at WCG-derived porous materials (Unpaired t-test, $p = 0.032$, $n = 6$).

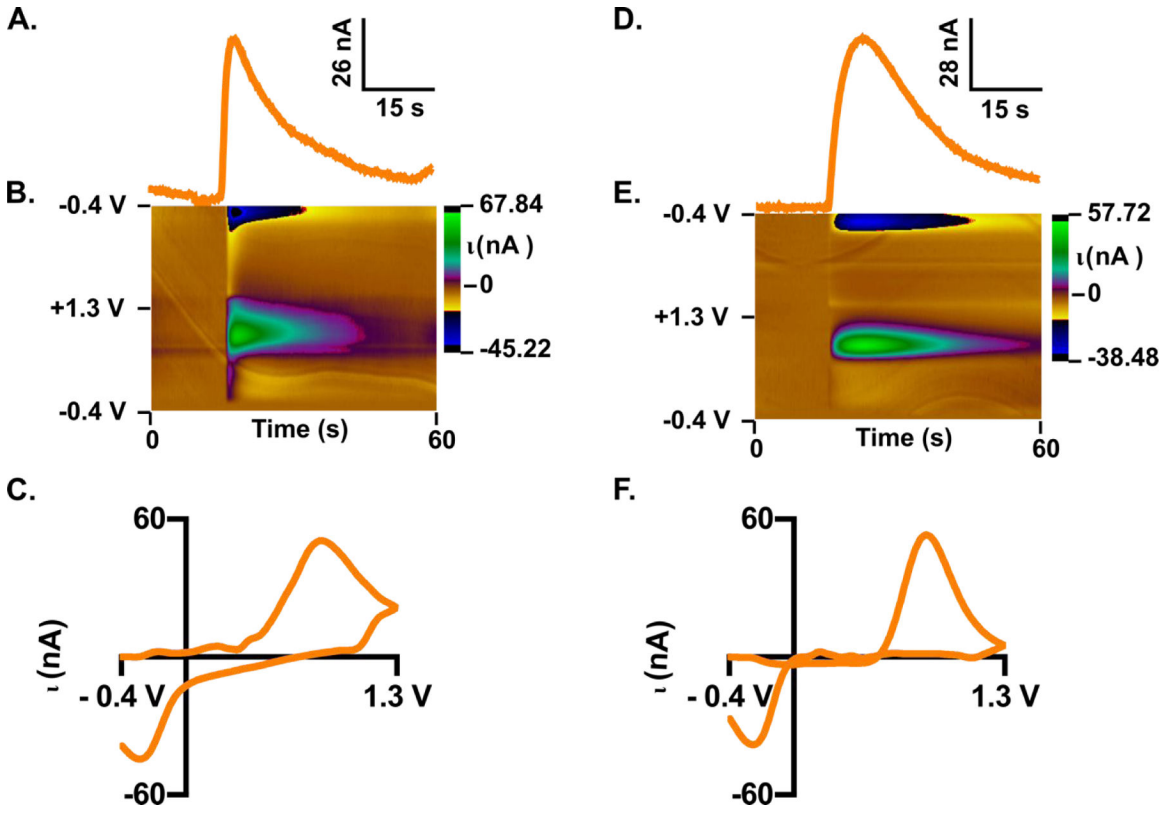

Figure 8.

Fast-scan cyclic voltammetry detection using WCG-modified CFMEs exhibit enhanced electrochemical reversibility in the mesenteric lymph node validating their utility making in-tissue measurements of catecholamines. (A) Current vs time trace of dopamine detected at a WCG-modified CFME after exogenous application of 25 μM dopamine. The corresponding false color plot (B) and cyclic voltammogram (C) are shown. (D) Current vs time trace of exogenous application of 25 μM norepinephrine detected at a WCG-modified CFME. The corresponding false color plot (E) and cyclic voltammogram (F) are shown.

Table 1:

Table summarizing synthetic parameters varied and their respective impacts on the degree of disorder and oxidative current enhancements for dopamine with FSCV.

Initial Heating (hr)	WCG:KOH	Final Heating (°C)	I_D/I_G ratio	Oxidation Current - Fold Increase
2	2:1	700	1.68 ± 0.06	1.4 ± 0.2
3	2:1	700	1.78 ± 0.08	[a] 2.3 ± 0.1**
3	1:2	700	1.85 ± 0.05	[b] 2.6 ± 0.2ns
3	1:2	900	1.73 ± 0.04	[c] 3.5 ± 0.4*

[a] Significant improvement in oxidation current with increasing the initial heating time (Unpaired t-test, p = 0.003, n=15).

[b] No significant increase in oxidation current with changing WCG:KOH ratio (Unpaired t-test, p = 0.23, n = 15).

[c] Significant improvement in oxidation current with increasing the final heating temperature (Unpaired t-test, p = 0.03, n = 15).

Table 2:

Comparison of capacitive current, sensitivity, limit of detection, redox cycling, and frequency dependence for bare and WCG-modified CFME

	i_c (nA)	**Sensitivity (nA μM^{-1})**	**LOD (nM)**	**Electrochemical Reversibility (τ_{ox}/ τ_{red})**	**Frequency Dependence**
Bare	1980 ± 210	9.8 ± 0.5	13.7 ± 5.0	2.2 ± 0.1	83.20 ± 0.04% loss
WCG-Modified	[a]2260 ± 210*	20.6 ± 1.6	[b]5.3 ± 2.0ns	[c]1.9 ± 0.1*	[d]63.62 ± 0.07% loss*

[a]Significant difference in capacitive current for bare and WCG-derived porous carbon modified CFMEs (Figure S8, paired t-test, p = 0.027, n = 15).

[b]No significant improvement in limit of detection due to added noise upon modification (unpaired t-test, p = 0.15, n=6).

[c]Significant improvement in redox cycling following porous carbon modification of CFMEs (paired t-test, p = 0.05, n=15).

[d]Significant improvement in frequency independence when modifying CFMEs with WCG-derived porous carbon (unpaired t-test, p = 0.032, n = 6).